An apropos kinematic framework for the numerical modelling of Friction Stir Welding

Narges Dialami, Michele Chiumenti, Miguel Cervera and Carlos Agelet de Saracibar

International Center for Numerical Methods in Engineering (CIMNE),

Technical University of Catalonia, Module C1, North Campus

C/ Gran Capitán s/n 08034 Barcelona, Spain.

Corresponding author: Narges Dialami

Tel.(+34) 93 401 6529 / Fax.(+34) 93 401 6517

E-mail addresses: narges@cimne.upc.edu (N. Dialami), michele@cimne.upc.edu (M. Chiumenti), mcervera@cimne.upc.edu (M. Cervera), agelet@cimne.upc.edu (C. Agelet de Saracibar)

Abstract

This paper describes features of a fully coupled thermo-mechanical model for Friction Stir Welding (FSW) simulation. An apropos kinematic setting for different zones of the computational domain is introduced and an efficient coupling strategy is proposed. Heat generation via viscous dissipation as well as frictional heating is considered.

The results of the simulation using the proposed model are compared with the experimental evidence. The effect of slip and stick condition on non-circular pin shapes is analyzed. Simulation of material stirring is also carried out via particle tracing, providing insight of the material flow pattern in the vicinity of the pin.

Keywords: Friction Stir Welding, Apropos kinematic framework, Particle tracing, Visco-plasticity, Friction, Stabilized finite element method

1. Introduction

1.1. The industrial process

FSW is a solid state joining technology in which no gross melting of the welded material takes place. It is a relatively new technique (developed by The Welding Institute (TWI), in Cambridge, UK, in 1991) widely used over the past decades for joining aluminium alloys. Recently, FSW has been applied to the joining of a wide variety of other metals and alloys such as magnesium, titanium, steel and others. This process offers a number of advantages over conventional joining processes (such as e.g. fusion welding). The main advantages include: (a) absence of the need for expensive consumables; (b) ease of automation of the machinery involved; (c) low distortion of the work-piece; and (d) good mechanical properties of the resultant joint [1]. Additionally being a solid state technique, it avoids all the problems associated to the cooling from the

liquid phase. Issues such as porosity, solute redistribution, solidification cracking and liquation cracking are not encountered during FSW. In general, FSW is found to produce a low concentration of defects and is very tolerant to variations in process parameters and materials. Furthermore, since welding occurs by the deformation of material at temperatures below the melting temperature, many problems commonly associated with joining of dissimilar aluminium alloys can be avoided, thus high-quality welds are produced. All these benefits render FSW appropriate for different industrial applications where metallurgical characteristics should be retained, such as in aeronautic, naval and automotive industry.

In FSW, a pin rotating at a constant speed is inserted into the welding line between two pieces of sheet or plate material (which are butted together) generating heat. This heat is produced by the *friction* between the pin shoulder and the work-pieces and by the mechanical mixing (*stirring*) in the solid state. The plasticized material is stirred by the pin and the heated material is forced to flow around the pin to its backside. There the material is consolidated to create a weld as the pin advances. As the temperature cools down, a solid continuous joint between the two plates emerges. Figure 1 shows the process schematically: The work-pieces joined by the weld are located on either the retreating or advancing side of the weld. The retreating side is the one where the pin rotating direction is opposite to the pin travel direction and parallel to the metal flow direction. In contrast, the advancing side is the one where the pin rotation direction is the same as the pin travel direction and opposite to the metal flow direction.

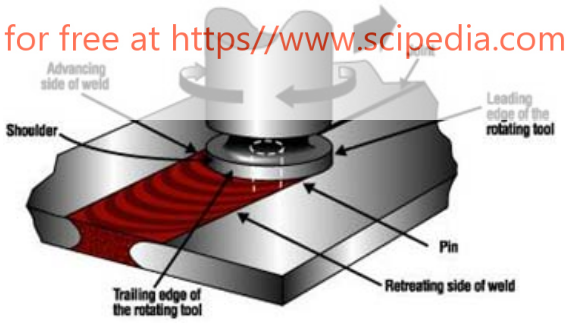

Figure 1: Friction Stir Welding schematic [2]

The numerical simulation is an important tool for understanding the mechanisms of the FSW process. It enables obtaining both qualitative and quantitative insights of the welding characteristics without performing costly experiments. Flexibility of the numerical methods (in particular FEM) in treating complex geometries and boundary conditions defines an important advantage of these methods against their analytical counterparts.

The FSW simulation typically involves studies of the transient temperature and its dependence on the rotation and advancing speed, residual stresses in the work-piece, etc. This simulation is not an easy task since it involves the interaction of thermal, mechanical and metallurgical phenomena. Up to now several researchers have carried out computational modelling of FSW. In the majority of the works, FSW process is studied at a *global* level. Simulation carried out at global level investigates the effect of moving heat source on the entire structure to be welded while *local* phenomena such as material flow are excluded. In a global approach, the generated heat is considered an input parameter. In different global studies various heat source types ranging from point sources to the distributed ones are considered. These studies typically analyze the effect of welding process on the structural behavior in terms of distortions, residual stresses or weakness along the welding line, among others.

Askari et al. [3] use the CTH finite volume hydrocode coupled to an advection-diffusion solver for the energy balance equation. Particular attention is given to the residual stresses in FSW joints in [4-6]. Giorgi et al. [5] study the effect of different shoulder geometries on the longitudinal stress distribution. Additionally, Dattoma et al. [6] investigate the influence of shoulder geometry on heat generation during the welding process. Chen and Kovacevic [7] use the commercial FEM software ANSYS for a Lagrangian finite element model of aluminium alloy AA-6061-T6. The welding pin is modeled as a heat source. This simple model severely limits the accuracy in the predicted stress and force, as the strain rate dependence is not included in the material model. However, the authors are able to investigate the effect of the heat moving source on the work-piece material.

Since the temperature is crucial for the FSW simulation, the heat source needs to be well-modeled. This consideration obliges to study the process at the *local* level where the simulation is concentrated on the stirring zone. For this type of simulation, the heat power is assumed to be generated either by the visco-plastic dissipation or by the friction at the contact interface. At this level the majority of the process phenomena can be analyzed: the relationship between rotation and advancing speed, the contact mechanisms, the effect of pin shape, the material flow within the heat affected zone (HAZ), the size of the HAZ and the corresponding consequences on the microstructure evolution, etc.

Among the local level studies, Cho et al. [8] use an Eulerian approach including thermo-mechanical models without considering the transient temperature in simulation. The strain hardening and texture evolution in the friction stir welds of stainless steel is studied in this paper. A Lagrangian approach with intensive re-meshing is employed in [9] while similar approaches are applied in [10, 11] which are not numerically efficient. Nandan et al. [12, 13] employ a control volume approach for discretization of the FSW domain. The material is considered as 3D visco-plastic flow to show the nature of

mass transportation in FSW. Assidi et al. [14] and Guerdoux [16] use an ALE formulation implemented into the commercial software with a splitting approach (one Lagrangian step followed by an advection phase), remapping techniques and an adaptive re-meshing scheme based on error estimation. Buffa el al. [15] predict the residual stresses in a 3D FE model for the FSW simulation of butt joints through a single block approach. The model is able to predict the residual stresses by considering only thermal actions.

Despite the wide range of FSW application in industry and related extensive research, many aspects of the process and of the ensuing mechanical properties are still not well-understood and require further studies. These include material mixing in the vicinity of the pin, influence of the pin shape and non-linear material behavior. The effort aimed at understanding the FSW process, such as computational modelling and simulation, is limited mainly because of the complexity of this thermo-mechanical process (e.g. material flow, temperature rise, large plastic deformation, contact and friction). Most of the existing models have limitations in either the representation of the non-circular pin geometries, or the non-linear material behavior, or application of the boundary conditions, or involve costly re-meshing procedure.

In this work we strive to develop a numerical tool for studying FSW at local level. The objective, however, is not to compromise on the computational efficiency and to develop a robust and efficient approach. One of the main objectives of the present work is to establish an apropos kinematic framework for the FSW simulation with arbitrary pin shapes together with an accurate definition of the boundary conditions. This framework allows to avoid remeshing and remapping of the state variables. Section 2 is explaining the division of the geometry into sub-domains and introduces an appropriate kinematic framework for each one of them. Coupling between each domain is detailed including the friction contact. As the heat due to plastic dissipation in FSW is usually large and cannot be neglected, mechanical and thermal equations become coupled thus necessitating a fully coupled thermo-mechanical model. Section 3 is devoted to the presentation of the coupled governing equations together with a rigid visco-plastic model suitable for the simulation of high deformation rate in FSW. Section 4 is devoted to particle tracing method applied for the visualization of material stirring around the pin. Section 5 is validating the work by simulation of some benchmarks and comparing them with experimental evidence.

2. Apropos Kinematic framework

In modelling FSW, the choice of kinematic frameworks for different domain zones (regions) crucially impacts the computational efficiency and the solution quality. For defining the suitable frameworks several observations must be made:

- The extent of the material deformation varies in different regions of the analysis domain.

- Pins used in practice are not necessarily circular.
- Boundary conditions must be applied conveniently.
- Re-definition of the integration domain and re-meshing is preferably to be avoided.

Considering these, the domain of the analysis is divided into three parts which are the Pin, the Plates and the heat affected zone (HAZ), associating a specific kinematic framework to each one of them.

Pin: The pin (Figure 2a) undergoes exclusively a rigid-body rotation at a constant speed and its deformation is not considered in the analysis. Thus, a Lagrangian framework is a natural choice for the description of the pin's movement.

Figure 2: Kinematic zones a) Pin b) HAZ c) Plate

HAZ: HAZ is a part of work-piece close to the pin where most of the material deformation takes place. The extent of the deformation in the vicinity of the pin is such, that it cannot be efficiently handled with a classical updated Lagrangian scheme, since it would lead to the mesh degradation and therefore necessity of a continuous re-meshing. At the same time, use of an Eulerian formulation would not be straight-forward for any pin shapes other than circular[1]. In the case of non-circular pins, additional techniques for tracking the moving boundary would be necessary as well as redefinition of the integration domain at every time step.

The ALE formulation allows overcoming the above mentioned problems provided a feasible mesh-moving strategy.

[1] The pin geometry influences the extent of mixing and thus the quality of the resulting weld.

Usually, using an ALE framework requires the treatment of the convective terms and the calculation of the mesh velocity following a splitting approach (see, for instance [14, 16]). There, the use of remeshing and remapping of state and internal variables are unavoidable.

In this work, HAZ is modeled as a circular region around the pin, as the flow there is predominantly rotational[2] (Figure 2b). The key idea consists in using the so-called *mesh sliding*, which in our case means rotating the HAZ mesh rigidly at each time step according to the pin movement, decoupling the material motion from the motion of the mesh. Consequently, the integration domain moves in such a way that the inner boundary of the HAZ is connected to the contour surface of the pin. Thus the ALE mesh velocity must be defined as:

$$\hat{v} = \omega \times R \tag{2.1}$$

where R is the distance between the given point and the center of rotation and ω is the angular velocity. With this choice of mesh velocity, the re-meshing in HAZ is avoided as the mesh does not undergo any deformations. Note that the material and the mesh motions are decoupled. Therefore, the convective term must be included in the governing equations, the convective velocity being equal to the difference between mesh and material velocity.

Plate: The area lying outside the HAZ is characterized by the material flow predominantly in the welding direction (Figure 2c). As in this area the domain neither changes its shape nor contains moving boundaries, the Eulerian framework can be used. The use of fixed mesh facilitates the application of boundary conditions on the inflow and outflow.

Coupling ALE and Eulerian parts: Coupling of the ALE (HAZ) and the Eulerian (welding plate) parts at the interface requires a special treatment as the mesh is fixed on one side (Eulerian) and moves on the other side (ALE). The coupling can be performed using a *node-to-node link* approach. The nodes lying at the interface are duplicated. At every mesh movement step the correspondence between the nodes belonging to the two parts (the plate and the HAZ) is established. For a given node of the ALE part the corresponding node of the Eulerian one is found[3] and a *link* between the two nodes is created (Figure 3). Afterwards, the boundary conditions and the properties of the plate nodes are copied to the corresponding HAZ nodes within the link. The time step must be chosen such that the two meshes (ALE and Eulerian) coincide at the interface. This means that the ALE mesh slides precisely from one Eulerian interface node to another at each time step. This requires having a coincident structured mesh at the mentioned interface.

[2] The domain must be chosen large enough to contain the whole deformation zone.
[3] This can be done by a nearest neighbor search.

The strategy proposed in this work is very advantageous from the point of view of computational efficiency, as it avoids remeshing and remapping of the variables. In this strategy, only the connection between the moving and the fixed parts changes at each time step; therefore, the moving mesh does not deform but slides.

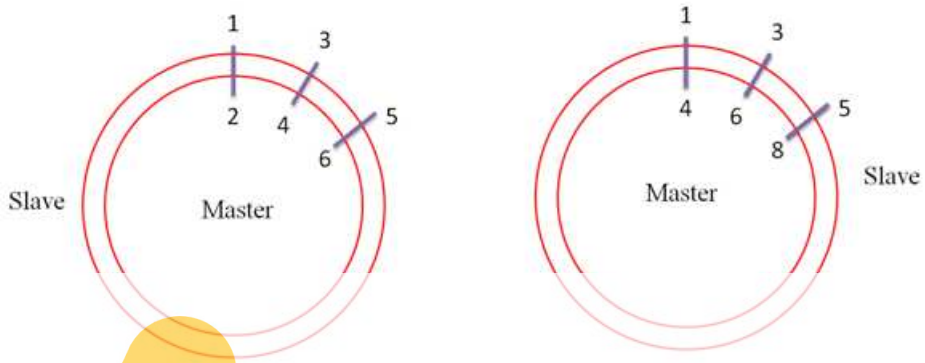

Figure 3: Coupling Ale and Eulerian parts

Coupling ALE and Lagrangian part: Coupling of the ALE (HAZ) and the Lagrangian (pin) parts at the interface requires a special attention too. While the mesh velocity in both cases is equal, the material velocities, the pressure and the temperature are different.

The contact between the pin and the HAZ material is generally characterized by slipping or nearly sticking condition. The corresponding boundary conditions applied at the pin/HAZ interface prescribe the material velocity field at the interface. The cases considered are modeled as follows:

- Full sticking: The local material velocity matching that of the pin everywhere at the interface.
- Slipping: The rotational speed of the material being an arbitrary constant fraction of the pin rotation speed.
- Stick/slip: Contact may be partially slipping and partially sticking, and if local melting occurs, there may be oscillating stick-slip behavior.

In this work, the frictional heating due to the contact interaction between pin/HAZ is defined by the Norton friction law [16]. Tangential (shear) component $\boldsymbol{t}_T$ of the traction vector at the contact interface is defined as

$$\boldsymbol{t}_T = a(T)\|\Delta \boldsymbol{v}_T\|^q \boldsymbol{u}_T \qquad (2.2)$$

where $a(T)$ is the (temperature dependent) material consistency and $0 \le q \le 1$ is the strain rate sensitivity. $\boldsymbol{u}_T$ is the tangential unit vector, $\boldsymbol{u}_T = \dfrac{\Delta \boldsymbol{v}_T}{\|\Delta \boldsymbol{v}_T\|}$ and $\Delta \boldsymbol{v}_T$ is the tangential component of the slip velocity.

3. Problem statement

In this section the coupled thermo-mechanical FSW model is introduced. The governing equations are formulated within the kinematic framework introduced in the previous section.

3.1. Mechanical model

For the FSW simulation, several assumptions are considered. First, the flow of the material around the pin is characterized by very low values of Reynolds number (Re<<1), typically around 10^{-4}, due to the very high viscosity of the material. For these values of Reynolds number, inertial effects and convection can be neglected. Thus a quasi-static analysis can be performed. Additionally, the flow can be considered incompressible as the volumetric changes including thermal deformation are found to be negligible.

Taking the above considerations into account and splitting the stress tensor $\boldsymbol{\sigma}$ into the volumetric and deviatoric parts,

$$\boldsymbol{\sigma} = p\mathbf{1} + \boldsymbol{s} \tag{3.1}$$

the mechanical problem (momentum and mass conservation) can be written as:

$$\nabla \cdot \boldsymbol{s} + \nabla p + \boldsymbol{f} = 0 \tag{3.2}$$

$$\nabla \cdot \boldsymbol{v} = 0 \tag{3.3}$$

where $\boldsymbol{v}$ and p are the velocity and the pressure. $\boldsymbol{f}$ and $\boldsymbol{s}$ are the body force and the stress deviator, respectively.

In FSW, the temperature gradient and the strain rate are very high in the vicinity of the pin requiring the use of rate-dependent constitutive models [17]. Several of these models are suitable for the simulation of FSW process. In the present work, the material behavior is modeled as rigid visco-plastic. In rigid visco-plastic models the constitutive equation is fully deviatoric. The relation between the stress deviator and the strain rate ($\dot{\boldsymbol{\varepsilon}}$) can be written as

$$\boldsymbol{s} = 2\bar{\mu}\dot{\boldsymbol{\varepsilon}} \tag{3.4}$$

Where the deformation rate ($\dot{\boldsymbol{\varepsilon}} = \nabla^s \boldsymbol{v}$) is the symmetric part of the velocity gradient and $\bar{\mu}$ is the effective viscosity coefficient of the material.

Based on the *Norton-Hoff* constitutive model, introduced originally by Norton [18] and extended by Hoff [19], the effective viscosity is expressed as

$$\bar{\mu} = \mu\left(\sqrt{3}\dot{\bar{\varepsilon}}\right)^{m-1} \tag{3.5}$$

where m and μ are the rate sensitivity and viscosity parameters respectively, both temperature dependent. $\dot{\bar{\varepsilon}}$ is the equivalent strain rate defined as

$$\dot{\bar{\varepsilon}} = \sqrt{2/3}\,\|\dot{\boldsymbol{\varepsilon}}\| = \sqrt{2/3}\,(\dot{\boldsymbol{\varepsilon}} : \dot{\boldsymbol{\varepsilon}})^{1/2} \tag{3.6}$$

In the present work the mechanical problem is solved using stabilized mixed linear $\boldsymbol{v}/p$ finite element formulation due to its good performance, especially for industrial simulations when triangular/tetrahedral meshes must be used for the domain discretization. The details on this formulation in the solid mechanics context can be found in [20-23].

3.2. Thermal model

The thermal problem is governed by the energy balance equation, which in ALE framework obtains the following form

$$\rho C_p \frac{\partial T}{\partial t} + \rho C_p \boldsymbol{v}^* \cdot \nabla T = -\nabla \cdot \boldsymbol{q} + \dot{D} \tag{3.7}$$

where $\boldsymbol{v}^* = \boldsymbol{v} - \hat{\boldsymbol{v}}$ is the convective velocity arising from the difference between material velocity $\boldsymbol{v}$ and mesh velocity $\hat{\boldsymbol{v}}$. ρ, C_p and T are the density, specific heat and the temperature, respectively. The last term $\dot{D}$ is the dissipation rate per unit of volume due to plastic deformation. The conductive heat flux $\boldsymbol{q}$ is defined according to the isotropic conduction law of Fourier as

$$\boldsymbol{q} = -k\nabla T \tag{3.8}$$

where k is the thermal conductivity.

The dissipation rate $\dot{D}$ depends on the plastic strain rate and the deviatoric stresses. Hence thermal and mechanical models become coupled [24, 25]. Therefore, the plastic dissipation $\dot{D}$ is defined as product of the deviatoric part of stress and strain rate:

$$\dot{D} = \gamma \boldsymbol{s} : \dot{\boldsymbol{\varepsilon}} \tag{3.9}$$

where γ is the plastic power fraction[4].

Thermal contact: Thermal exchange by conduction between the work-piece and the pin takes place at the contact surface interface. This is expressed by the following equation:

[4] Around 90% of the plastic dissipation is converted into heat [26].

$$-k\nabla T \cdot \boldsymbol{n} = h_{cond}\left(T - T_{pin}\right) \tag{3.10}$$

where h_{cond} is the conduction coefficient, $\boldsymbol{n}$ is the unit vector normal to the surface, T is temperature of the work-piece and T_{pin} is the pin temperature in contact with the work-piece.

At the free surfaces, convection and radiation heat fluxes responsible for heat loss to the environment must be considered. The thermal exchange with the environment due to convection can be computed using Newton's law:

$$-k\nabla T \cdot \boldsymbol{n} = h_{conv}\left(T - T_{env}\right) \tag{3.11}$$

where h_{conv} is the convection heat transfer coefficient and T_{env} is the surrounding environment temperature.

The radiation heat flux is governed by the Stefan–Boltzmann law, which is a function of the surface temperature, T and T_{env}:

$$-k\nabla T \cdot \boldsymbol{n} = \sigma_0 e\left(T^4 - T_{env}^4\right) \tag{3.12}$$

where σ_0 is the Stefan–Boltzmann constant and e is the emissivity factor.

The thermal problem is solved using a linear stabilized finite element formulation in space and Backward Euler time integration scheme in time.

4. Tracers

In the FSW process, the plastic deformation is extremely high in the vicinity of the pin. Thus, the material stirring/mixing is encountered in that area. The extent of material mixing plays a critical role for the weld quality and the joint-strength. To produce a high quality and defect-free weld, it is essential to get an insight of the material deformation path due to mixing. However, it is difficult to observe this path directly in the solid-state. Several experimental and numerical techniques for predicting the material flow can be applied. Experimentally, the motion of the stirred material is usually tracked using the Marker Insert Technique (MIT). The markers are embedded into the path of rotating pin[5] and their final position after welding is detected by metallographic means.

In the numerical simulation, to visualize the trajectories of material particles due to stirring, a *particle tracing* technique can be used. Particle tracing is a method generally used to simulate the motion of large number of particles and track their trajectories. Therefore, it can be naturally applied to the simulation of the material flow around the pin in FSW. A set of

[5] In practice, they are placed at different position at the center line.

nodes (not forming part of the computational mesh) is introduced in the area to be analyzed (Figure 4). These nodes represent the material particles to be tracked and are called *tracers*.

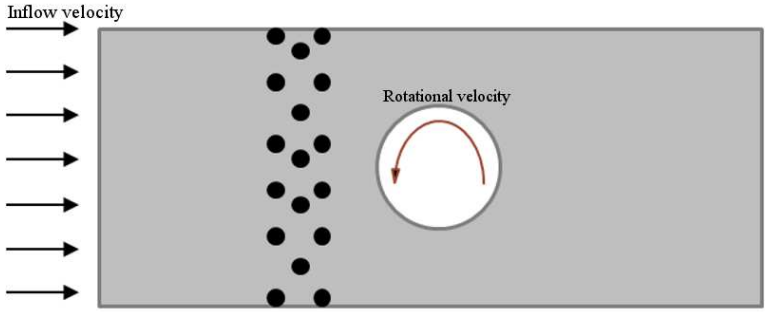

Figure 4: Particle distribution

The trajectories of the tracers are computed from the velocity field obtained at the end of each time step (purely Post-Processing step) as

$$\frac{D(X(t))}{Dt} = V(X(t),t) \tag{4.1}$$

with initial conditions $X = X_0; t = t_0$, where $X(t)$ is the position of the tracer at time t and $V(X(t),t)$ is the velocity of the tracer in the position $X(t)$ and time t.

The ordinary differential equation (4.1) must be solved for each individual particle. Its solution (a sequence of particle's positions $(X(t_0), X(t_1),...)$) defines the trajectories of the stirred material. It can be solved by any conventional time integration methods (e.g. Forward Euler and Backward Euler).

In this work a *sub-stepping* method is used as it is found to give superior results without leading to a computational overhead. According to the sub-stepping method, the particle position of the time step $n+1$ is computed in k sub-steps (Figure 5) as:

$$\begin{cases} \boldsymbol{X}_{n+1} = \boldsymbol{X}_n + \int_{t_n}^{t_{n+1}} \boldsymbol{V}_{n+1} \mathrm{d}t \cong \boldsymbol{X}_n + \sum_{i=1}^{k} \boldsymbol{V}_{n+1}^{i} \delta t^i \\ \Delta t = \sum_{i=1}^{k} \delta t^i \end{cases} \tag{4.2}$$

where Δt is the time step, δt^i is the i^{th} sub-step.

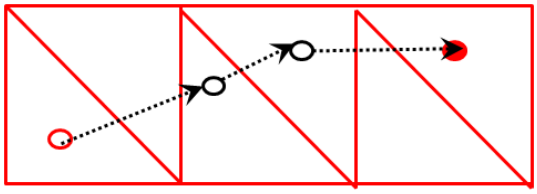

Figure 5: Particle movement at each sub-step

As the velocity is known only at the mesh nodes, the velocity of the particles must be found via interpolation of the nodal values of the corresponding element. At each sub-step a spatial search algorithm must be performed in order to find the elements containing the particles. Once the element containing a given particle is found, corresponding values of the shape functions are computed to obtain the sub-step velocity $\boldsymbol{V}_{n+1}^{i}$ as

$$\boldsymbol{V}_{n+1}^{i}=\sum_{j=1}^{3}\left(\boldsymbol{v}_{n+1}^{i}\right)^{j} N^{j}\left(\boldsymbol{X}_{n+1}^{i}\right) \tag{4.3}$$

where $N^{j}\left(\boldsymbol{X}_{n+1}^{i}\right)$ is the shape function at the particle position.

The nodal velocities $\boldsymbol{v}_{n+1}^{i}$ at sub-steps are unknown and thus need to be approximated from nodal velocities at time n and $n+1$ as well as the nodal displacements[6].

$$\begin{cases} \boldsymbol{v}_{n+1}^{i}(t)=(1-\tau_t)\boldsymbol{v}_n+\tau_t\boldsymbol{v}_{n+1} \\ \boldsymbol{x}_{n+1}^{i}(t)=(1-\tau_t)\boldsymbol{x}_n+\tau_t\boldsymbol{x}_{n+1} \\ \tau_t=\dfrac{(t-t_n)}{(t_{n+1}-t_n)} \quad t_n<t<t_{n+1} \end{cases} \tag{4.4}$$

5. Numerical simulations

In this section three examples are chosen in order to show:

- The validity of the method by comparing the result of a 3D simulation with the experimental results.
- The suitability of the proposed kinematic framework for the simulation of noncircular pins under slip and stick condition
- The performance of the proposed particle tracing method by comparison with experimental evidence.

5.1. 3D FSW with circular pin

[6] As the ALE approach is chosen for the area close to the pin, the nodal positions vary between sub-steps and needs to be updated.

This example is a 3D simulation of FSW process. Geometry data, process parameters and material properties used in the simulation are taken from [14, 27] and served for comparing their experimental results with the numerical ones obtained in this work.

A cylindrical pin is considered in the analysis. The pin (Figure 6) is 8 *mm* in diameter and its depth inside of the plate is 6.35 *mm*. The pin shoulder is 25.4 *mm* in diameter with a shoulder concavity angle of 8º and the height of the pin is 90 *mm*. The work-pieces have 300 *mm* length in the welding direction 150 *mm* width in the transversal direction and a thickness of 9.53 *mm*. Back-plate has the same 300 *mm* length, 150 *mm* width as work-piece but a thickness of 25 *mm*.

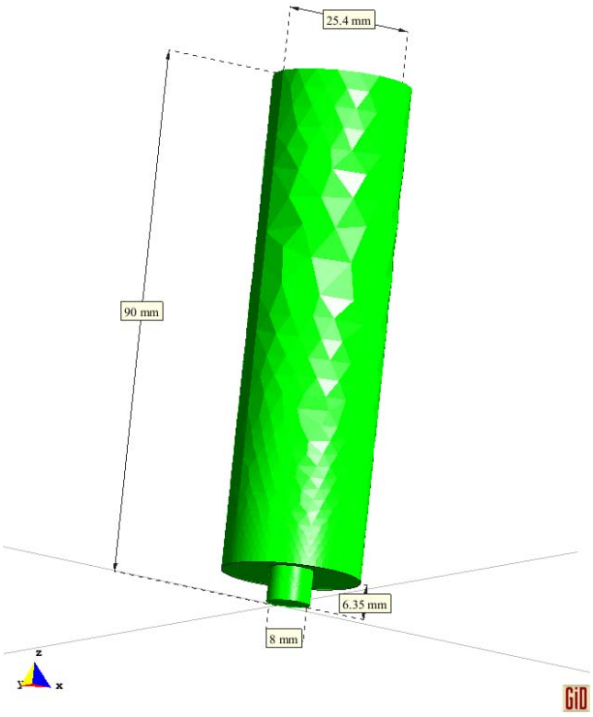

Figure 6: Geometry information of the pin

The welding speed and rotational velocity of the pin are $V_s = 3.39$ *mm/s* and $V_r = 650$ *RPM*, respectively. The rotational velocity is prescribed as a constant tangential velocity at the pin volume. In the simulation, convection-radiation heat transfer to the ambience, heat conduction between the pin and the work-piece, work-piece and back-plate are taken into account. Heat generation through plastic dissipation and friction is considered. In the simulation, the initial and environmental temperatures are 20ºC.

The material used for the back-plate located underneath the work-piece is Al 6061-T6. The pin and the work-piece are made of steel and Al 6061, respectively. A *Norton-Hoff* constitutive law is used for the work-piece (Figure 7) while pin and the back-plate are simulated as thermo rigid materials (Table 1). Thermal material properties for work-piece, back-plate and pin are presented in Table 2.

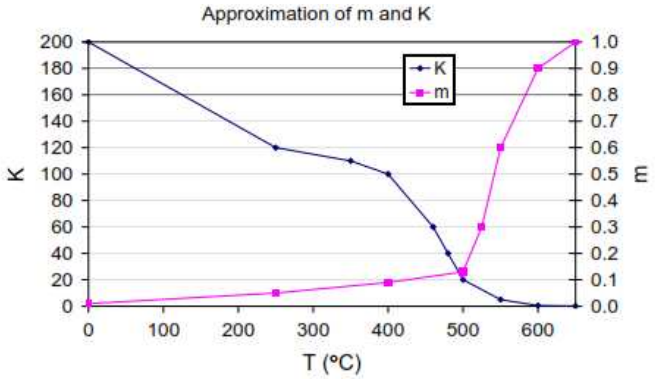

Figure 7: Norton-Hoff material properties [14]

Parts	Material	Constitutive model
Work-piece	Al6061	Norton-Hoff
Pin	Steel	Rigid
Back-plate	Al6061-T6	Rigid

Table 1: Materials and constitutive laws

Parts	ρ (Kg/m^3)	C_p(J/kgºC)	k(W/mºC)	e
Work-piece	2700	896	180	0.05
Pin	7850	460	24.3	0.88
Back-plate	2800	1230	250	0.05

Table 2: Thermal properties

The geometry is discretized with a mesh consisting of 59630 linear tetrahedral elements and 11157 nodal points (Figure 8). Figure 9 shows a magnified view of the mesh discretization for the pin and the work-piece.

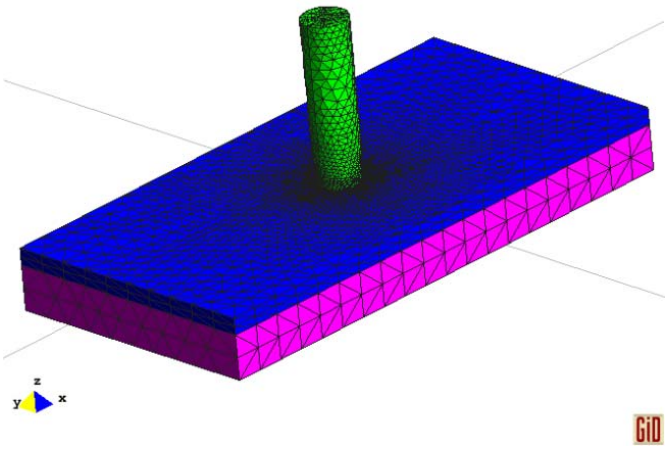

Figure 8: Finite Element mesh

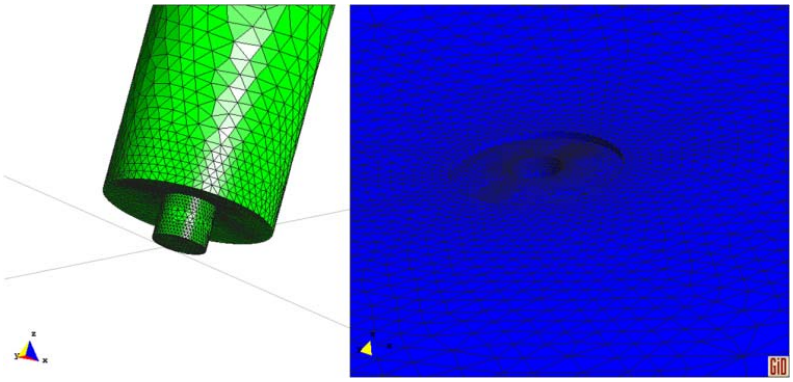

Figure 9: Finite Element mesh in detail for pin and work-piece

The temperature contour field at the end of the simulation is shown in Figure 10. The heat near the pin can only dissipate throughout the work-piece which leads to a continuous increase of temperature farther away from the pin. In reality, heat also goes into the backing plate. More in detail, Figure 11 shows a cross section of the pin, work-piece and the back plate. The temperature field is compared with the one obtained from [14] at time 60*s*. Very high temperature in the thickness direction of the work-piece under the pin shoulder is observed. Note that because of the strain rate concentration and sharp temperature gradient in the vicinity of the pin and shoulder, a refined mesh must be used in this area.

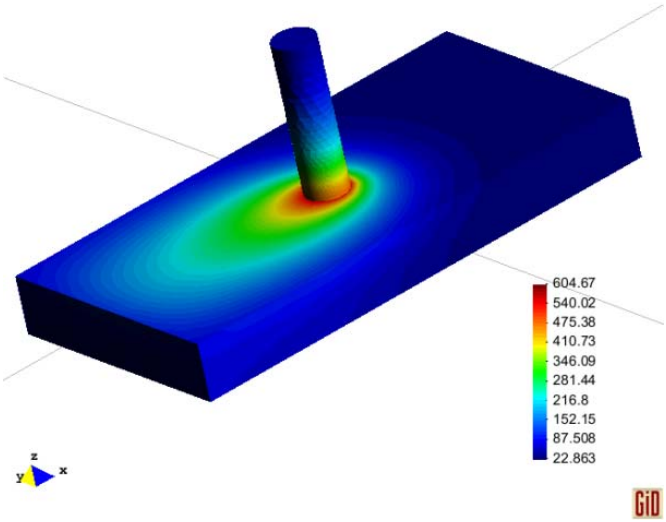

Figure 10: Temperature contour field at the end of simulation

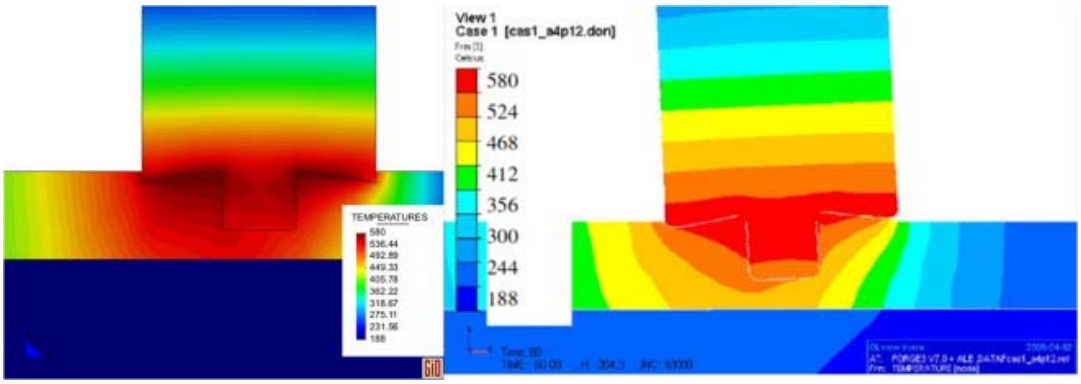

Figure 11: Temperature contour field on the cross section in welding line

The results obtained exhibits asymmetry of the temperature profiles around the pin because of the rotational and linear motion of the pin and asymmetry of heat generation around the pin surface.

Figures 12 compare the experimental results reported by Guerdoux [27] and the numerical results obtained in the current work. The temperature is indicated for 3 different parts of the tool which are the pin, the shoulder and the root. It can be seen that the numerical results are in a very good agreement with the experimental ones.

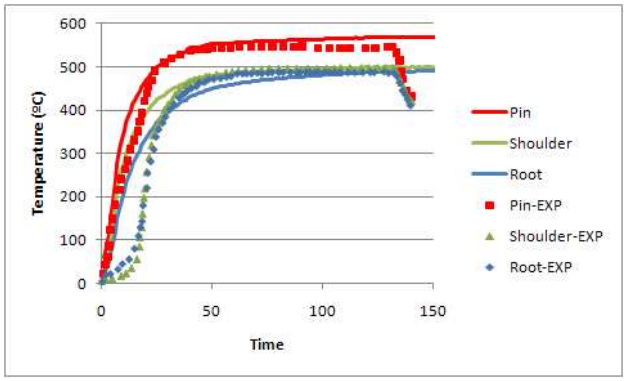

Figure 12: Temperature evolution compared with experiment on pin, shoulder and root

5.2. 3D FSW with a Trivex pin

In this example a plate and a pin with the same dimension as the one in section 5.1 are considered. The cross section of the pin is trivex. The Trivex pin design is approximately triangular; the three points of the pin form an equilateral triangle with the side lengths 6.93 *mm* and are connected by convex sides of 73º (Figure 13).

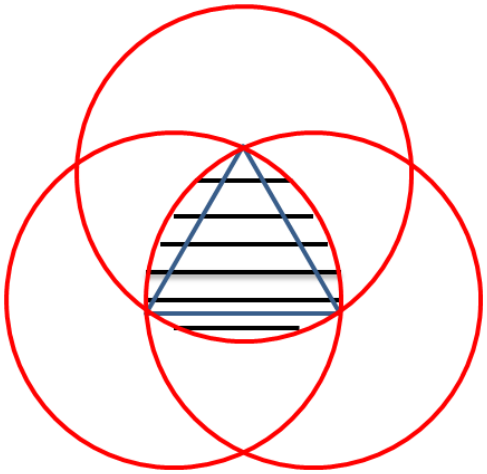

Figure 13: Geometry of a trivex

The contact conditions between the pin and the material are central to the FSW process. The objectives of this example are on one side, to study the effect of slip and stick boundary conditions on the temperature field at the contact interface and on the other side, to show the ability of the proposed method for the simulation involving non circular pins. The applied inflow velocity is 3.39 *mm/s* while the rotational pin velocity is 650 *RPM*.

The Norton-Hoff material constitutive law is assumed with constant parameters and the thermal properties summarized in the section 5.1.

The Figures 14 shows the temperature contour field on the trivex pin, ALE zone and plate. The uniform temperature field is obtained due to the heat generated by the plastic dissipation as a result of the material stirring and the friction at the pin/HAZ interface.

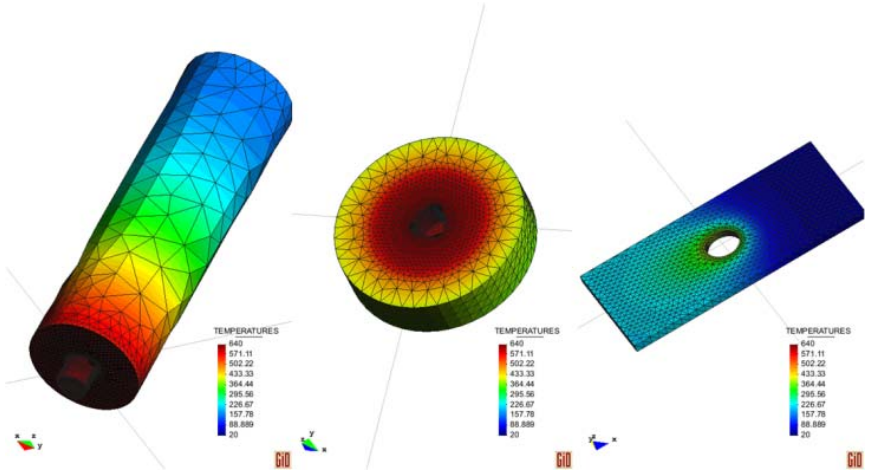

Figure 14: Temperature field from left to right on trivex pin, ALE zone and Plate

Figure 15 illustrates the temperature contour field for the fully stick, slip/stick and fully slip conditions, respectively. In the stick case, the material is stuck to the rotating pin, which leads to a higher strain rate and temperature than if the material is allowed to slip.

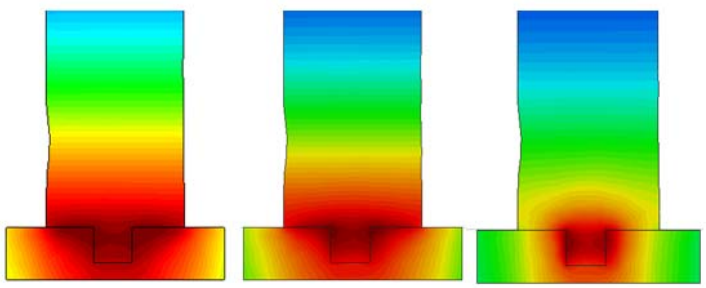

Figure 15: Temperature contour field from left to right with fully stick, stick/slip and fully slip condition.

5.3. Particle tracing (2D case)

This example uses the processing conditions and pin geometry described in the work of Seidel and Reynolds [28], where experimental evidence of the particle tracing is provided.

A pin used is of 9.9 mm in diameter which is a cross section of the threaded bolt perpendicular to the axis.

Process parameters are: welding speed V_s = 5.0833 *mm/sec*, rotational speed V_r = 500 *RPM* and room temperature $T_0 = 25\,^{\circ}C$. The welding plate's material is Aluminum AA2195-T8.

Figure 16 shows the final position of the particles, which is computed at mentioned rotational and translational speeds. Material from the retreating side is transported along with the rotating pin to the advancing side. Some parts of the material move even to the backward direction. Advancing side material is mainly transported backwards. The connection of advancing and retreating side behind the pin is not necessarily located at the centerline.

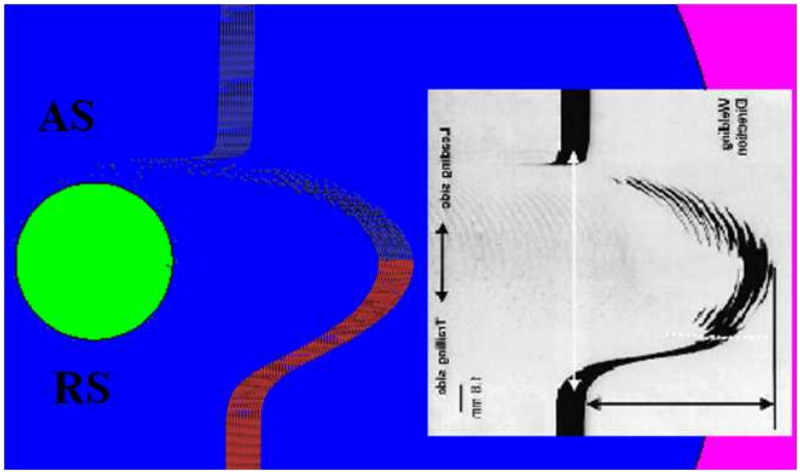

Figure 16: Tracer visualization, simulation (left) experiment (right)

The model is discretized with a mesh of 4986 triangular elements. Despite the fact that this 2D model does not consider vertical flow produced by the thread, the results show that the numerical particle tracing can reveal characteristic patterns of material flow in FSW. On the advancing side a flow pattern with *sawing* shape is seen, which qualitatively correlates with the experimental data. This result is encouraging and prompted us to construct a three dimensional model.

6. Summary and conclusions

In the current paper, a thermo-mechanical model for FSW simulation is proposed. Thermal analysis is assumed to be transient while a quasi-static approximation is used for the mechanical problem.

The apropos kinematic framework based on the combination of ALE, Eulerian and Lagrangian descriptions proposed in this work for different parts of the computational domain is found to be advantageous. It allows treating arbitrary pin geometries and conveniently applying the boundary conditions. A mesh moving strategy chosen for the ALE part of the domain facilitates coupling with the rest of the sub-domains (Lagrangian and Eulerian ones).

A *Norton-Hoff* rigid thermo-visco-plastic constitutive equation is used to characterize the material. The thermal contact and heat convection-radiation through the boundaries are considered. Heat generated by plastic dissipation and friction is taken into account. The effect of slip and stick boundary conditions is studied.

The material stirring is simulated by means of particle tracing method. The trends observed are consistent with the results of experiments, showing motion of markers inserted into the weld.

In spite of the inherent complexities of the friction stir welding modelling (including constitutive and transient heat equations, various boundary conditions, etc.), the obtained numerical results provide some confidence that the method proposed here is a promising numerical tool for simulating FSW. This paper demonstrates the capability of the proposed numerical model to efficiently simulate different types of material flows that are encountered in FSW, and accurately compute the resulting thermo-mechanical fields.

References

[1] S. M. Packer, T. W. Nelson and C. D. Sorensen, Tool and equipment requirements for friction stir welding ferrous and other high melting temperature alloys, The 3rd International Symposium on Friction Stir Welding, Kobe, Japan, 2001.

[2] P. Dong, F. Lu, J. Hong and Z. Cao, Analysis of Weld Formation Process in Friction Stir Welding, The 2nd International Symposium on Friction Stir Welding. Gothenburg, Sweden, 2000.

[3] A. Askari, S. Silling, B. London and M. Mahoney, Modelling and Analysis of Friction Stir Welding Processes, The 4th International Symposium on Friction Stir Welding, GKSS Workshop, Park City, Utah, USA, 2003.

[4] M. B. Prime, T. Gnäupel-Herold, J. A. Baumann, R. J. Lederich, D. M. Bowden and R. J. Sebring, Residual stress measurement in a thick, dissimilar aluminum alloy friction stir weld, Acta Materialia 54 (2006) 4013 – 4021.

[5] M. De Giorgi, A. Scialpi, F. Panella and L. De Filippis, Effect of Shoulder Geometry on Residual Stress and Fatigue Properties of AA6082 FSW Joints, Journal of Mechanical Science and Technology, 23 (2009), 26-35.

[6] V. Dattoma, M. De Giorgi and R. Nobile, On the residual stress field in the Aluminium alloy FSW joints, Strain 45 (2009) 380–386.

[7] C. Chen and R. Kovacevic, Thermomechanical modelling and force analysis of friction stir welding by the finite element method, Proc. Inst Mech. Eng., Part C: J. Mech. Eng. Sci., 218 (2004) 509–519.

[8] J. Cho, D. Boyce and P. Dawson, Modelling strain hardening and texture evolution in friction stir welding of stainless steel, Materials Science and Engineering, A398 (2005) 146–163.

[9] J.L. Chenot and E. Massoni, Finite element modelling and control of new metal forming processes, Journal of Machine Tools and Manufacture, 46 (2006) 1194–1200.

[10] G. Buffa, J. Hu, R. Shivpuri and L. Fratini, Design of the friction stir welding tool using the continuum based FEM model, Materials Science and Engineering A419 (2006) 381–388.

[11] Buffa, G., Hu, J., Shivpuri, R. and L. Fratini, A continuum based fem model for friction stir welding-model development, Materials Science and Engineering A419 (2006) 389–396.

[12] R. Nandan, G. G. Roy, T. J. Lienert and T. DebRoy, Numerical modelling of 3D plastic flow and heat transfer during friction stir welding of stainless steel, Science and Technology of Welding and Joining 11 (2006) 526-537.

[13] R. Nandan, G. G. Roy, T. J. Lienert and T. DebRoy, Three-dimensional heat and material flow during friction stir welding of mild steel, Acta Materialia 55 (2007) 883–895.

[14] M. Assidi, L. Fourment, S. Guerdoux and T. Nelson, Friction model for friction stir welding process simulation: calibrations from welding experiments, Int. J. Mach. Tools Manuf. 50 (2) (2010) 143–155.

[15] G. Buffa, A. Ducato And L. Fratini, Numerical procedure for residual stresses prediction in friction stir welding, Finite Elements in Analysis and Design 47 (2011) 470–476.

[16] S. Guerdoux and L. Fourment , A 3D numerical simulation of different phases of friction stir welding, Modell. Simul. Mater. Sci. Eng. 17 (2009) 075001.

[17] P. Ulysse, Three-Dimensional Modelling of the Friction Stir Welding Process, International Journal of Machine Tools and Manufacture, 42 (2002) 1549-1557.

[18] F.H. Norton, The creep of steel at high temperature. Mc Graw Hill, New York, USA, 1929.

[19] H. J. Hoff, Approximate Analysis of structures in presence of moderately large creep deformation Quart. Appl. Math 12 (1954) 49-55.

[20] C. Agelet de Saracibar, M. Chiumenti, Q. Valverde and M. Cervera, On the orthogonal subgrid scale pressure stabilization of finite deformation J2 plasticity, Comp. Method in Appl. Mech. and Eng. 195 (2006) 1224-1251.

[21] M. Chiumenti, Q. Valverde, C. Agelet de Saracibar and M. Cervera, A stabilized formulation for elasticity using linear displacement and pressure interpolations, Comp. Meth. in Appl. Mech. and Eng. 191 (2002) 5253-5264.

[22] M. Chiumenti, Q. Valverde, C. Agelet de Saracibar and M. Cervera, A stabilized formulation for incompressible plasticity using linear triangles and tetrahedra, Int. Journal of Plasticity 20 (2004) 1487-1504.

[23] M. Cervera, M. Chiumenti, Q. Valverde and C. Agelet de Saracibar, Mixed linear/linear simplicial elements for incompressible elasticity and plasticity, Comp. Method in Appl. Mech. and Eng. 192 (2003) 5249-5263.

[24] C. Agelet de Saracibar, C. Cervera and M. Chiumenti, On the formulation of coupled thermoplastic problems with phase-change, International journal of plasticity 15 (1999) 1-34.

[25] C. Cervera, C. Agelet de Saracibar and M. Chiumenti, Thermo-mechanical analysis of industrial solidification processes, Int. J. Numer. Meth. Eng. 46 (1999) 1575-1591.

[26] W. Johnson and H.K. Kudo, The Mechanics of Extrusion, Manchester University Press, Manchester, UK, 1962.

[27] S. Guerdoux, Numerical simulation of the friction stir welding process, ParisTech, 2007.

[28] T. U. Seidel and A.P. Reynolds, Visualization of the material flow in AA2195 Friction Stir Welds using a marker insert technique, Metallurgical and Materials Transaction A32 (2001) 2879-2884.